

1 Covalent Protein Painting Reveals Structural Changes in the Proteome in
2 Alzheimer Disease

3 Casimir Bamberger ^{1*}, Sandra Pankow ^{1*}, Salvador Martínez-Bartolomé ¹, Michelle Ma ¹,
4 Jolene Diedrich ¹, Robert A. Rissman ^{2,3} and John R. Yates III ¹

5

6 * contributed equally

7 Addresses:

8 ¹ Department of Molecular Medicine, The Scripps Research Institute, 10550 North Torrey Pines
9 Road, La Jolla, CA 92037, USA.

10 ² Department of Neurosciences, University of California San Diego, 9500 Gilman Drive,
11 La Jolla, CA 92093, USA.

12 ³ Veterans Affairs San Diego Healthcare System, San Diego, CA, 92161, USA.

13

14

15

16 To whom correspondence should be addressed:

17 John Robert Yates III
18 10550 North Torrey Pines Road, SR302
19 The Scripps Research Institute
20 La Jolla, CA 92037
21 United States

22

23 Abstract

24 The 3D structures of aberrant protein folds have been visualized in exquisite detail, yet no
25 method has been able to quantitatively measure protein misfolding across a proteome. Here,
26 we present Covalent Protein Painting (CPP), a mass spectrometry-based structural proteomics
27 approach to quantify the accessibility of lysine ϵ -amines for chemical modification at the
28 surface of natively folded proteins. We used CPP to survey 2,645 lysine residues in the
29 proteome of HEK293T cells *in vivo* and found that mild heat shock increased rather than
30 decreased lysine accessibility for chemical modification. CPP was able to differentiate patients
31 with Alzheimer disease (AD) or Lewy body disease (LBD) or both from controls based on relative
32 accessibility of lysine residues K147, K137, and K28 in Tubulin- β , Succinate dehydrogenase, and
33 amyloid- β peptide, respectively. The alterations of Tubulin- β and Succinate dehydrogenase
34 hint to broader perturbations of the proteome in AD beyond amyloid- β and hyper-
35 phosphorylated tau.

36
37
38
39
40
41
42
43
44
45
46
47
48
49

50 Keywords

51 Protein surface mapping, neurodegenerative diseases, bottom-up proteomics, MudPIT, isobaric
52 isotopologue, mass defect, quantitative mass spectrometry, structural proteomics, diffuse Lewy
53 body disease, conformational diagnostics, molecular diagnostics, conformational diagnostics.

54 Introduction

55 AD is a neurodegenerative disorder marked by progressive loss of cognition and other
56 important mental functions. While the cause for AD remains unclear, age is the strongest risk
57 factor for its onset ([https://www.alz.org/alzheimers-dementia/what-is-alzheimers/causes-and-](https://www.alz.org/alzheimers-dementia/what-is-alzheimers/causes-and-risk-factors)
58 [risk-factors](https://www.alz.org/alzheimers-dementia/what-is-alzheimers/causes-and-risk-factors)). A breakdown of the blood-brain barrier and continuous neuronal cell death
59 contributes to cognitive and behavioral decline in AD patients ¹. The deposition of
60 neurofibrillary tangles and senile plaques precede neuronal cell death and are disease defining
61 hallmarks of AD ². Tangles consist of macromolecular aggregates of tau protein whereas
62 plaques mainly contain aggregated amyloid- β peptide. However, neuronal cell death is not
63 linked to amyloid- β fibril formation in tauopathies or in dementias with Lewy bodies, which
64 yield large aggregates of tau protein and α -synuclein, respectively. While the onset and
65 progression of these neurodegenerative diseases differ, they are all characterized by an
66 accumulation of misfolded proteins. Cells normally recognize proteins with incorrect folds and
67 attempt to re-fold or to pass them on to proteasomal degradation. Chaperone proteins like
68 heat shock proteins play a key role in recognizing misfolded proteins and in refolding client
69 proteins. Chaperones are part of the proteostasis network which encompasses a highly diverse
70 group of proteins that keep the proteome in homeostasis ³. If the proteostasis network fails to
71 recognize and remove misfolded proteins, conformationally altered proteins accumulate and
72 can cause cell death. In age correlated neurodegenerative diseases additional changes might
73 impinge on protein conformation homeostasis and it is tempting to propose an insufficiency in
74 removing misfolded proteins with increasing organismal age as a molecular explanation for the
75 onset of neurodegeneration. However, the large number of protein conformations and
76 interactions present in cells makes it experimentally challenging to trace and pinpoint where,
77 when, and why specific proteins misfold and persist in a misfolded state.

78 In an initial step to monitor protein conformer homeostasis we attempted to measure the
79 degree of protein misfolding *in vivo*. We therefore developed Covalent Protein Painting (CPP),
80 a structural proteomics approach to quantify changes in protein fold or altered protein-protein
81 interaction for any protein in a proteome. CPP directly determines the relative surface
82 accessibility of amino acid side chains by measuring the molar fraction of a chemical

83 functionality that is accessible for chemical modification on the surface of proteins. Here, we
84 targeted the ϵ -amine of lysine which is a primary amine. Instead of assessing changes in 3D-
85 structure with *in vitro* labeling techniques like “rates of oxidation” (SPROX) ^{4,5}, we adopted a
86 standard formaldehyde-based tissue fixation protocol ⁶ to dimethylate all lysine ϵ -amines that
87 are sufficiently solvent exposed to be chemically modified. Dimethylation leaves a smaller
88 chemical footprint than other chemically more complex reagents used for *in vitro* labeling of
89 lysine residues in highly purified protein complexes such as succimidylanhydride ⁷,
90 diethylpyrocarbonate ⁸, or “Tandem Mass Tags” (TMT) ⁹.

91 In CPP, solvent exposed primary amines are chemically dimethylated with very high yields
92 within seconds because the addition of each methyl moiety is a two-step reaction that is only
93 rate limited by the initial formation of the hydroxymethylamine ¹⁰. Subsequently, the labeling
94 reaction is quenched, labeling reagents are removed, and proteins are denatured and
95 proteolytically digested with an endoprotease that is insensitive to lysine. The remaining,
96 previously non-accessible lysine residues which become accessible as a result of proteolysis are
97 labeled in a second labeling step with a set of isotopically different dimethyl moieties. When
98 measured with mass spectrometry, this label allows CPP to directly determine the fraction of
99 protein molecules that was accessible for chemical modification at a specific lysine site based
100 on the relative intensities of the isotope labeled peptides that include that site. The covalent
101 attachment of the label and its *in vivo* applicability sets CPP apart from other approaches for
102 determining protein structure, such as Protein Painting which non-covalently “coats” the
103 protein’s surface with small molecules in order to limit tryptic cleavage ¹¹ or limited proteolysis
104 which takes advantage of a differential availability of amino acid sequences for non-specific
105 proteolytic digestion ¹². Like other methods, CPP enables an unbiased discovery of structural
106 changes caused by misfolding and altered protein-protein interactions in cells and tissues.

107 Using CPP we show that heat shock of HEK293T cells preferentially increased surface
108 accessibility of lysine sites for chemical modification and that it significantly altered surface
109 accessibility at 14 of 2,645 different lysine sites. Finally, we used CPP to differentiate between
110 patients with neurodegenerative diseases and controls based on an altered lysine accessibility

111 in Tubulin- β , Succinate dehydrogenase, and amyloid- β peptide in postmortem collected brain
112 tissue samples.

113 Results

114 3D proteome with CPP

115 We used $^{13}\text{CH}_3$ isotope-defined formaldehyde and sodium cyanoborohydride to dimethylate
116 solvent exposed lysine ϵ -amines in the proteome of HEK293T cells *in vivo* (Figure 1A and
117 Extended data figure 1, Materials and Methods). Proteins were denatured and digested with
118 the lysine-insensitive endoprotease Chymotrypsin. After digestion newly exposed primary
119 amines in peptides were dimethylated with CDH_2 formaldehyde and sodium
120 cyanoborodeuteride. Following reversed-phase chromatography of peptides, mass spectra of
121 peptide fragment ions were acquired in highest resolution (R 120,000) on an Orbitrap Fusion
122 mass spectrometer in order to differentiate and quantify $^{13}\text{CH}_3$ from CDH_2 -labeled
123 peptides ¹³. Despite the reduced scan speed of the mass spectrometer at its highest resolution
124 settings, CPP surveyed 385 lysine residues in 246 different proteins with 2,297 individual
125 measurements from a total of six replicate experiments which included exchange of isotope
126 and alternative combinations between the first versus second labeling step (first : second label,
127 $\text{CDH}_2 : ^{13}\text{CH}_3$, $^{13}\text{CH}_3 : \text{CDH}_2$, $^{13}\text{CHD}_2 : \text{CD}_3$, $\text{CD}_3 : ^{13}\text{CHD}_2$). Each measure of relative abundance of
128 the first to the second isobaric label at a lysine site yielded a ratio R per lysine site ¹³. R values
129 were converted into percentiles of relative accessibility ($\% \text{ accessibility} = 100 * R / (1 + R)$)
130 which reflects the proportion of protein or proteoform molecules in which a specific lysine site
131 was accessible for chemical modification.

132 Consistent with lysine being the most solvent accessible amino acid in proteins, initial
133 dimethylation labeled 337 out of 385 lysine sites (87.5 %) in > 95 % of protein or proteoform
134 molecules. The remaining 47 lysine sites were either completely inaccessible (13 sites) or
135 accessible in \leq 95 % of protein molecules (34 sites, Extended data table 1). Several different
136 lysine sites of the metabolic enzyme Glyceraldehyde 3-phosphate dehydrogenase GAPDH were
137 quantified in the dataset and lysine sites GAPDH#K27, GAPDH#K55, and GAPDH#K139 were
138 measured as completely accessible in all GAPDH molecules. In contrast, lysine residue
139 GAPDH#K309 was accessible for chemical modification in < 75 % of GAPDH molecules

140 (Figure 1B). Crystal structures of GAPDH show that GAPDH#K309 is participates in the protein-
 141 protein interface of two homo-dimers within the GAPDH homo-tetramer ¹⁴ (Figure 1C,
 142 Extended data figure 2).
 143 Additional *in vitro* experiments showed that GAPDH#K309 was accessible in < 20 % (and
 144 conversely, inaccessible in > 80 %) of recombinantly expressed, highly purified human GAPDH
 145 tetramers whereas an additional 13 lysine sites were solvent exposed in, on average, 97 % of

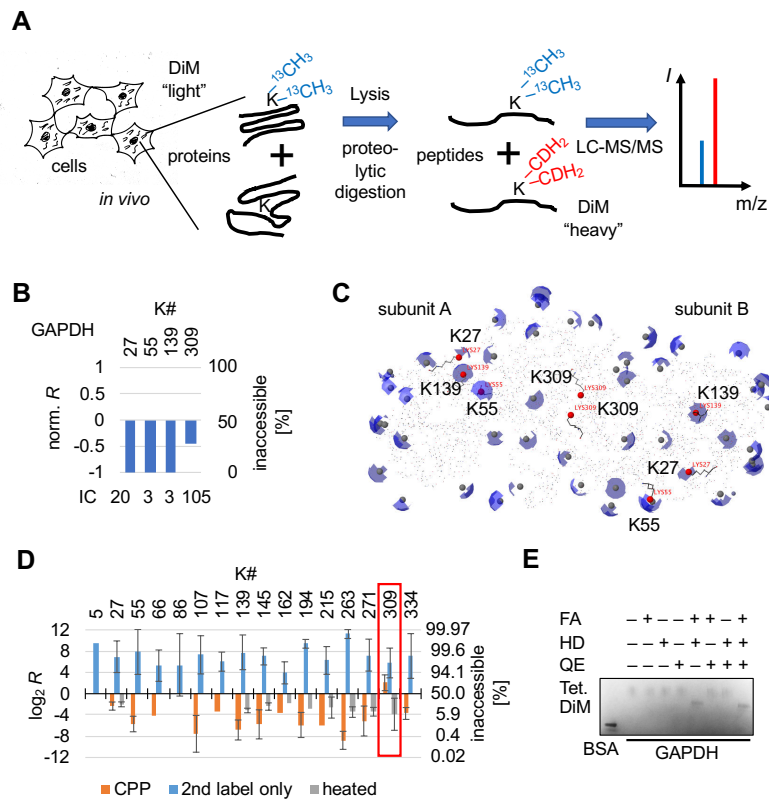


Figure 1 Covalent Protein Painting (CPP) determines whether the ϵ -amino group of lysine is accessible for chemical modification. (A) The schematic displays the workflow of CPP. Reductive alkylation labels lysine residues in proteins with isotope-defined "light" dimethyl moieties in cells *in vivo*. Following digestion into peptides with a lysine-insensitive protease (Chymotrypsin), newly solvent exposed lysine residues are modified with isotope-defined "heavy" dimethyl moieties. Bottom up mass spectrometry is used to analyze the ratio of light to heavy isotope labeled peptide molecules per lysine site. (B) Lysine residue K309 of human GAPDH is only partially accessible for chemical dimethylation in HEK293T cells. Proteins in HEK293T cells were covalently modified with CPP using isobaric isotopologue methyl moieties with $^{13}\text{CH}_3$ for light and CDH_2 for heavy, and the relative surface accessibility determined as described in (A). Numbers above the bars indicate the position of the lysine residue in GAPDH. The y-axis is the ratio of light to heavy fragment ion counts normalized to the total number of ion counts shown below each bar. A ratio of $R = 1:1$ ($\log_2(1) = 0$) indicates that the lysine site was accessible for chemical modification in 50 %, $R > 0$ in > 50 %, and $R < 0$ in < 50 % of protein molecules. Ion counts (IC) denotes the sum of fragment ion peaks. (C) One GAPDH dimer of the homo-tetramer (PDB: 4wnc) is displayed. Partial spheres (blue) highlight solvent accessible surface area (SASA) of each individual lysine ϵ -amine (grey sphere). Lysine residues that were assayed with CPP are highlighted in red in (B). GAPDH#K309 resides within the contact surface of two GAPDH monomers in the GAPDH dimer. (D) The bar graph shows accessibility of different GAPDH lysine sites for chemical dimethylation in highly purified, native GAPDH tetramers (orange), heat denatured GAPDH (grey), and when the initial labeling step was omitted. A red box highlights CPP results obtained for GAPDH#K309. (E) Blue-native gel electrophoresis of GAPDH indicates stability of the homo-tetramer following chemical dimethylation. GAPDH was pre-incubated with labeling reagents formaldehyde (FA), sodium cyanoborohydride (HD), and the quencher ammonium bicarbonate (QE). Bovine serum albumin (BSA, 66 kD) was included as molecular size indicator. Tetrameric GAPDH protein complexes migrated distinctively faster following CPP. Error bars are standard deviation (σ). Abbreviations: DiM, dimethyl moieties; Tet., homo-tetramers.

146 GAPDH molecules ($\sigma = \pm 1.8$ of $\log_2 R$, Figure 1D and Extended data Figure 3). The remaining 12
147 of 26 total lysine sites in GAPDH were either not detected or peptides harbored more than one
148 lysine residue upon endo-proteolytic digestion with Chymotrypsin which precluded a site-
149 specific quantitation based on chromatographic elution profiles ¹⁵.

150 Next, we tested whether CPP detected protein unfolding and misfolding. Purified human
151 GAPDH was heat denatured (95 °C, 5 min) and subjected to CPP. All lysine residues, including
152 GAPDH#K309, were now accessible in at least > 80 %, and on average in 87 % ($\sigma = \pm 0.7$, $\log_2 R$)
153 of GAPDH molecules (Figure 1D, grey bars). Heat denaturation overall lowered lysine
154 accessibility from 97 % of molecules in native GAPDH to 87 % suggesting that random protein
155 aggregation following heat denaturation rendered lysine residues inaccessible in 10% of protein
156 molecules. As an additional control, we omitted the first labeling step, endoproteolytically
157 digested non-modified GAPDH, and dimethylated all lysine residues (Figure 1D, blue bars). As
158 expected, in this control lysine sites were accessible for labeling on average in 99.3 % ($\sigma = \pm 1.9$,
159 $\log_2 R$) of GAPDH molecules as expected. The residual 0.7% reflected most likely random
160 chemical noise picked up during mass spectrometric data acquisition and quantification of
161 elution profiles.

162 Native gel electrophoresis showed that chemical dimethylation did not affect the tertiary
 163 structure of GAPDH (Figure 1E). Dimethylated GAPDH homo-tetramers (147 kD) migrated as a
 164 sharp signal slightly below non-modified GAPDH homo-tetramers but well above bovine serum
 165 albumin (BSA, 66.5 kD). The molecular weight of BSA is close to the calculated molecular
 166 weight of GAPDH dimers that were not observed. The signal intensity did not diminish,
 167 suggesting that GAPDH tetramers did not disassemble upon dimethylation. A comparison of
 168 the results to the solvent accessible surface area (SASA) of lysine ϵ -amines in crystal structures
 169 of GAPDH indicated that ϵ -amines required a SASA of $> 1 \text{ \AA}^2$ in order to be chemically modified
 170 with CPP. Because the CPP results were congruent with the actual fold and tertiary structure of
 171 GAPDH and based on the results of additional experiments (Supplementary Information), we

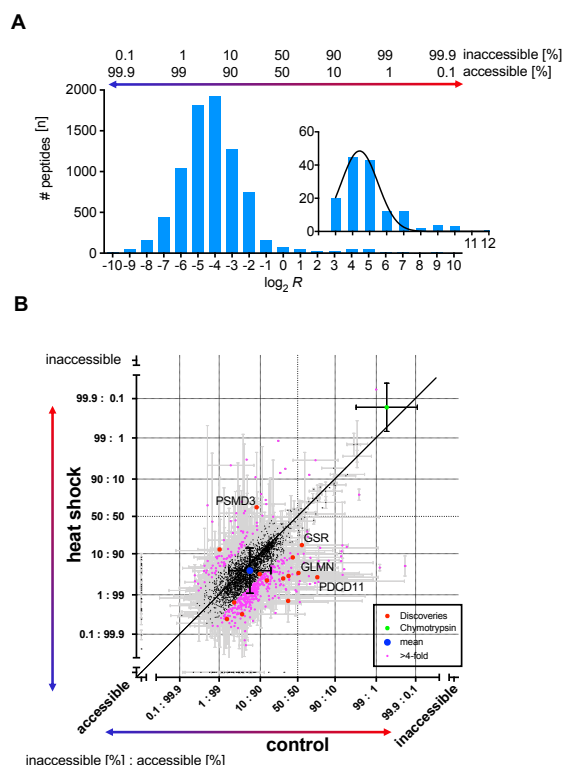


Figure 2 CPP quantified protein unfolding in HEK293T cells upon mild heat shock *in vivo*. (A) The frequency plot shows the distribution of the relative proportion of protein molecules in which a lysine site was accessible for chemical modification with CPP in the proteome of HEK293T cells. $\log_2 R$ values were binned by integer and the frequency distribution of lysine sites inaccessible for chemical modification in a majority of protein molecules are highlighted in the inset. The black line is a Gaussian fit. The relative number of protein molecules [%] in which lysine sites were accessible to chemical modification is indicated on top of the bar graph. (B) The scatterplot compares the relative number of protein molecules in which a lysine residue was accessible for chemical modification in control to heat shock-treated HEK293T cells. The units “accessible” and “inaccessible” on the scale bar indicate lysine sites that were measured as either completely accessible or inaccessible in control or heat shock. Pink dots highlight individual lysine residues that differed between heat shock and control by $\Delta > 2$. Dots in red indicate lysine sites that passed the discovery threshold of $q < 0.01$. CRBT1#K54 in Chymotrypsin is highlighted in green and the overall mean shown in blue. The 45° angled line (black) denotes no change between control and heat shock. Error bars are standard deviation (σ).

172 conclude that CPP measures the proportion of protein molecules in which a specific lysine
173 residue was accessible for chemical modification.

174 A rise in temperature from 37 °C to 42 °C for 15 min is a physical stress that leads to protein
175 unfolding or misfolding in eukaryotic cells and elicits a coordinated cellular response of the
176 proteostasis network to limit proteome-wide damage¹⁶. We applied CPP to HEK293T cells
177 *in vivo* to find out whether heat preferentially misfolds a specific subset of proteins or whether
178 it leads to wide-spread random unfolding of proteins in the proteome. We used
179 multidimensional protein identification technology (MudPIT)¹⁷ on an Orbitrap Velos mass
180 spectrometer to survey the proteome in three biological replicates of HEK293T control cells
181 following heat shock (42 °C, 15 min). The experiment yielded 16,081 different peptide
182 measurements covering a total of > 7,000 different lysine sites of which 2,645 were quantified
183 at least twice per condition in 979 different protein groups and proteoforms (Extended data
184 table 2).

185 2,484 of 2,645 lysine residues were accessible for chemical modification in > 33 % of protein
186 molecules in control HEK293T cells (Extended data figure 4 and Extended data
187 network 1). Individual lysine sites were accessible for labeling in 94.4 % of protein molecules on
188 average and accessibility normally distributed from 99.7 % to 50 % (2σ -interval of Gaussian fit,
189 $R^2 = 0.9958$, Figure 2A). The remaining 161 lysine residues that were accessible for chemical
190 modification in ≤ 33 % of protein molecules clustered in a distinct second peak in the frequency
191 distribution plot (Figure 2A Inset). A positive control in CPP represents the exogenously added
192 endoprotease Chymotrypsin that was not present during initial labeling. Following proteolytic
193 digestion, endoproteolytic peptides of Chymotrypsin are labeled in the second labeling step
194 only, and thus none of its peptides can be quantified as accessible for chemical
195 modification. Lysine residue K54 of the endoprotease Chymotrypsin (CRBT1#K54) was
196 measured as “accessible” in 0.16 % of molecules most likely due to random chemical noise in
197 mass spectra.

198 Heat shock altered relative surface accessibility in 461 of 2,645 lysine sites by $> \sigma$ (≥ 4 -fold, pink
199 dots in the scatter plot in Figure 2B) and these lysine sites were more likely to become more

200 accessible (369 sites) than inaccessible (92 sites) for chemical modification, indicating that heat
201 shock preferentially unfolded proteins or weakened protein-protein interactions. Notably, the
202 fractional change in the number of protein molecules with increased accessibility was < 20 %
203 for the majority of the 369 lysine sites (Extended data figure 5). Thus, CPP revealed that most
204 proteins are likely reversibly unfolded upon heat shock, reflecting increased entropy in the
205 HEK293T proteome at elevated temperatures.

206 Heat shock not only preferentially increased the relative proportion of protein molecules in
207 which a lysine site was accessible, it also significantly altered accessibility for chemical
208 modification in 14 lysine sites (q -value < 0.01, red dots in the scatter plot in Figure 2B). For 4 of
209 the 14 proteins, heat shock flipped the proportion of protein molecules from predominantly
210 accessible (> 50 %) to inaccessible (< 50 %) for chemical modification or vice versa (Extended
211 data table 3). K273 in the 26S proteasome non-ATPase regulatory subunit 3, PSMD3,
212 (PSMD3#K273) was the only lysine site in the dataset which was accessible in the majority of
213 PSMD3 molecules in control (91.7 %) and ended up accessible in only 36.8 % of PSMD3
214 molecules upon heat shock. All three additional lysine sites turned from predominantly
215 inaccessible to accessible in > 50 % of protein molecules upon heat stress. PDCD11#K1402 in
216 programmed cell death protein 11 (RRP5 homolog NF κ B binding protein, NFBP) shifted from
217 accessible in 24.0 % to accessible in 97.3 % of PDCD11 molecules upon heat shock. In
218 mitochondrial Glutathione reductase, GSR, lysine site GSR#K501 changed from accessible in
219 43.9 % to accessible in 84.3 % of GSR molecules, and GLMN#K507 in Glomulin turned from
220 accessible in 49.9 % to accessible in 96.5 % of GLMN molecules upon heat exposure. In
221 summary, CPP revealed that mild heat shock increases entropy in the proteome based on a rise
222 in the number protein molecules in which lysine was accessible for chemical modification. In a
223 few proteins, heat shock led to alterations in protein conformation or protein-protein
224 interaction that were potentially irreversible.

225 Prolonged heat shock causes extensive post translational protein modifications (PTM) on
226 lysine, including ubiquitinylation and sumoylation¹⁸. Thus, we determined if ubiquitinylation
227 and sumoylation in response to heat shock occurred at lysine sites that were also quantified by
228 CPP. 68 proteins were either ubiquitinylated or sumoylated in control and heat shock-exposed

229 cells, with more PTM occurrences following heat shock. Ubiquitinated or sumoylated proteins
230 were overall enriched for the Gene Ontology term “protein folding” (p -value = 12.9), and
231 several ubiquitinylation sites were identified with > 5 spectral counts (SpC) across all biological
232 replicates, including tubulin- α (TBA1B, 13 SpC), splicing factor (U2AF2, 13 SpC), and
233 heterogeneous nuclear ribonucleoprotein R (HNRNPR, 9 SpC), and apoptosis inhibitor 5 (API5,
234 5 SpC). Proteins ubiquitinated only in heat shock-exposed cells included the ubiquitin-like
235 modifier-activating enzyme 1 (UBA1, 13 SpC), transcription intermediary factor 1 β (TRIM28,
236 8 SpC), and heat shock 70 kD protein (HSP70, 5 SpC). Overall, CPP covered 20 proteins and
237 lysine sites out of 68 proteins that were ubiquitinated or sumoylated. Differences in
238 accessibility for chemical dimethylation were below 2-fold for most of these lysine sites. An
239 exception was lysine site TBA1B#K430 in Tubulin- α 1B, which was sumoylated upon heat shock
240 and showed 3.4-fold more TBA1B molecules that were inaccessible for chemical
241 dimethylation. Likewise, TPIS1#K256 in triosephosphate isomerase 1 was sumoylated and
242 displayed 3.8-fold more TPIS1 molecules in which TPIS1#K256 was inaccessible after heat
243 shock. PTM modification does not necessarily decrease the proportion of molecules in which
244 PTM modified lysine site was accessible for chemical modification; HSP74#K84 of heat shock
245 protein 70 kD protein 4 was inaccessible in 3.6-fold less HSP74 molecules despite being
246 ubiquitinated upon heat shock. As expected, a subset of lysine sites quantified with CPP were
247 also PTM modified. CPP does not quantify changes in PTM because CPP tests only non PTM-
248 modified lysine residues. One exception is naturally occurring lysine dimethylation, which can
249 influence CPP results depending on the choice of isotope-defined reagents used in the design of
250 the experiment (Supplementary Information).

251 Differentiating neurodegenerative diseases based on 3D alterations
 252 Next, we tested CPP as a potential conformational diagnostic tool to measure protein
 253 misfolding in neurodegenerative diseases. We analyzed prefrontal cortex samples of
 254 10 controls and 10 patients that were diagnosed with AD, LBD or with severe diffuse LBD in
 255 addition to AD (AD-dLBD, Extended data table 4). CPP was applied to whole tissue lysate and to
 256 the pellet formed following ultracentrifugation (UC) to enrich for protein aggregates¹⁹. Overall,
 257 the experiment quantified 559, 342, and 303 lysine sites in lysate, pellet, and supernatant,
 258 respectively. Only lysine sites in amyloid precursor protein APP, APP#K699, mitochondrial
 259 succinate dehydrogenase SDHB, SDHB#K137, and tubulin- β TUBB, TUBB#K174 were
 260 significantly altered between controls and AD, AD-dLBD or LBD in the lysate (q -value < 0.05,

Table 1

Diagnosis	Sample	Ab#K28				SDHB#K137		TUBB#K174	
		Lysate		Pellet		Lysate		Lysate	
		SpC	%acc	SpC	%acc	SpC	%acc	SpC	%acc
AD	A10	2	89	2	99	0	n.d.	2	98
AD	A7	4	79	7	92	2	58	1	99
AD	A4	7	65	5	92	4	56	1	99
AD-dLBD	A6	4	75	5	94	2	58	2	98
AD-dLBD	B10	7	84	6	94	2	62	2	98
AD-dLBD	B6	6	51	7	86	2	61	1	98
AD-dLBD	A9	6	49	5	82	1	72	1	99
AD-dLBD	B7	7	48	8	51	2	60	2	99
AD-dLBD	B8	6	62	5	84	1	56	2	97
LBD	B5	0	n.d.	0	n.d.	2	57	2	98
Normal	A1	0	n.d.	0	n.d.	0	n.d.	2	99
Normal	A2	0	n.d.	0	n.d.	0	n.d.	1	98
Normal	A3	0	n.d.	0	n.d.	2	91	1	99
Normal	A5	0	n.d.	0	n.d.	0	n.d.	2	99
Normal	A8	0	n.d.	0	n.d.	0	n.d.	1	99
Normal	B1	0	n.d.	0	n.d.	1	80	1	99
Normal	B3	0	n.d.	0	n.d.	2	80	2	99
Normal	B9	0	n.d.	0	n.d.	0	n.d.	1	99
Normal	B4	0	n.d.	0	n.d.	2	79	2	99
Normal	B2	3	7	1	4	2	78	2	99

Table 1 Amyloid- β misfold in AD and LBD patient prefrontal cortex. The table shows the accessibility in percent for Ab#K28 and SDHB#K137, and TUBB#K174 lysine sites in 10 patient and 10 control samples. Note that Ab#K28 was not detected in the supernatant following UC in any of the samples whereas it was present in UC pellet as well as initial lysate of patients diagnosed with AD. Abbreviations: SpC, spectrum count; %acc, percentile of peptide or protein molecules in which the lysine site was accessible for chemical dimethylation.

261 Table 1). TUBB#K174 was overall accessible in 99.2 % to 97.3 % tubulin- β molecules. In AD, AD-
 262 dLBD and LBD samples TUBB#K174 was on average accessible for chemical modification in
 263 0.6 % fewer molecules than in controls. SDHB#K137 was on average accessible for chemical

264 modification in 21.4 % fewer protein molecules in AD, AD-dLBD, and LBD. Inaccessibility for
265 chemical modification increased > 2-fold in patient-derived samples over controls, in which
266 SDHB#K137 was measured in half of all samples.

267 Lysine site K699 in a chymotryptic peptide of APP was almost exclusively present in AD and AD-
268 dLBD samples. APP is the precursor protein of amyloid- β peptides $A\beta_{1-40}$ and $A\beta_{1-42}$ which are
269 the naturally occurring endoproteolytic cleavage products of APP that form large peptide
270 aggregates or plaques in AD patients²⁰. APP#K699 matches $A\beta$ #K28 in the amyloid- β peptides
271 $A\beta_{1-40}$ and $A\beta_{1-42}$. We infer chymotryptic APP#K699 peptides were derived from naturally
272 accumulated amyloid- β peptides rather than from APP for a number of reasons. First,
273 additional peptides that matched APP only and not amyloid- β peptides $A\beta_{1-40}$ and $A\beta_{1-42}$ were
274 not detected in any of the samples. Second, peptides were present only in lysate and UC pellet
275 but not UC supernatant, suggesting that only aggregated proteins or peptides yielded sufficient
276 amounts of chymotryptic cleaved $A\beta$ peptide for mass spectrometric detection. Third, $A\beta$
277 peptides were not detected in an LBD only patient sample which is consistent with the
278 observation that $A\beta$ plaques are absent in LBD only diseased patients. Fourth, peptides
279 originating from $A\beta$ were not detected in 9 out of 10 control samples from cognitively
280 unimpaired patients in any of the three different sample preparations (lysate, UC pellet and UC
281 supernatant). The only control sample in which peptides originating from $A\beta$ were detected
282 was B2 where $A\beta$ #K28 was detected and inaccessible for chemical modification in almost all
283 chymotryptic peptide molecules. We further consider sample B2 as outlier because it was
284 derived from an individual who did not show symptoms of neurodegeneration. $A\beta$ #K28
285 accessibility varied between 48 % and 89 % in the brain tissue lysate AD and AD-dLBD patient
286 samples. $A\beta$ #K28 was accessible between 65 % to 89 % of peptide molecules in patients
287 diagnosed with AD only whereas it was accessible between 48 % to 75 % of peptide molecules
288 in patients diagnosed with AD-dLBD. Thus, in AD-dLBD patients $A\beta$ #K28 was on average
289 accessible in fewer (but not significantly fewer) molecules than in AD only patient samples.
290 Biochemical purification of protein aggregates impacted CPP results. $A\beta$ #K28 was consistently
291 accessible for chemical modification in more peptide molecules in the UC pellet than in the

292 lysate. The largest fold difference in peptides with inaccessible A β #K28 was observed in AD
293 patient sample A10 in which the percentage of peptide molecules with accessible A β #K28
294 increased from 89 % in the lysate to 99 % in the UC pellet. Thus, the proportion of peptide
295 molecules in which A β #K28 is inaccessible for chemical modification changed > 10-fold, from
296 11 % to 1 % in sample A10. For all samples, fold changes measured after UC correlated with the
297 initial accessibility in lysate or remained almost unaltered when the number of peptide
298 molecules with accessible A β #K28 was \geq ~50 % in the lysate: AD-dLBD patient B7 showed
299 A β #K28 lysine accessibility for chemical modification in 48 % of peptide molecules in Lysate and
300 51 % of peptide molecules in UC, and control B2 in 7 % and 4 % of peptide molecules in lysate
301 and UC pellet, respectively. These differences show that UC can increase the proportion of A β
302 peptide molecules in which A β #K28 was accessible for chemical dimethylation.

303 Discussion

304 Here, we demonstrated the feasibility and versatility of covalent protein painting, CPP, to
305 measure changes in chemical reactivity of lysine sites across a complete proteome in HEK293T
306 cells *in vivo*. Mild heat shock unfolded or disrupted protein-protein interactions in < 20 % of
307 protein molecules. This increase in the number of protein molecules with lysine sites accessible
308 for chemical modification most likely reflects increased entropy in the proteome at higher
309 temperatures. Lysine sites in three proteins, PDCD11, GSR, and GLMN switched from
310 predominantly inaccessible to predominantly accessible (> 90 %) which suggests that this
311 change was non-random, and thus might identify these proteins as molecular thermostats with
312 a non-linear response to heat shock. The molecular pathways associated with these proteins
313 are ribosome assembly (PDCD11), oxidative stress response (GSR), and protein translation
314 (GLMN). PDCD11 supports maturation of ribosomal subunits 40S and 80S ²¹ and processing of
315 47S rRNA ²² which transiently subsides during prolonged heat shock ²³. GLMN binds to RBX1
316 and prevents E2 ligase recruitment and therewith Cul1 E3 ligase-mediated ubiquitinylation of
317 substrates ²⁴. However, GLMN#K507 does not map to the interaction surface of GLMN with
318 RBX1 ²⁴ indicating that heat shock disrupts a protein-protein interaction or protein
319 conformation that is not further characterized.

320 Utilizing CPP as a conformational diagnostic tool we found that A β #K28 in amyloid- β ,
321 TUBB#K147 in TUBB, and SDHB#K137 in SDHB were less accessible for chemical modification in
322 patients with neurodegenerative disease than in controls. While the difference for TUBB#K147
323 was small (0.6 %), it might still be of biological relevance because microtubules directly support
324 neuronal function. SDHB is part of the oxidative respiration chain in mitochondria which is a
325 key metabolic process that fails in aging neurons. A 2-fold increase in molecules with altered
326 accessibility to lysine site SDHB#K137 might reflect a previously unidentified alteration in SDHB
327 protein structure or protein-protein interaction in AD. Previous work showed that the
328 dehydrogenase activity of SDHB is blocked by amyloid- β peptide ²⁵.

329 Misfolding and aggregation of amyloid- β peptide is a key molecular signature of AD that is
330 intensely studied. In brief, a number of non-imaging techniques coupled to mass spectrometry
331 were used to determine the amyloid- β misfold *in vitro* such as hydroxyl radical protein
332 footprinting ²⁶ and fast photochemical induction of hydroxyl radicals" (FPOP) ²⁷, which oxidizes
333 amino acid moieties on the surface of a limited number of proteins ²⁸. Hydrogen-deuterium
334 exchange coupled with mass spectrometry (HDX-MS) ²⁹ revealed surface exposed hydrogen
335 atoms of fibrillar amyloid- β with high spatial resolution *in vitro* ³⁰ and reductive alkylation of
336 amyloid- β protein fibrils in combination with peptide based-mass spectrometry ³¹ or limited
337 proteolysis followed by mass spectrometry ³² also elucidated the structural constraints of lysine
338 residues in *in vitro*-assembled amyloid- β fibrils. The structure of amyloid- β fibrils was first
339 revealed in AD patient brain samples with light and later electron microscopy ^{33,34}, and x-ray
340 diffraction showed that amyloid- β fibrils consist of amyloid- β peptides that fold into two anti-
341 parallel β -strands that associate in a short β -sheet secondary structure or "pleated sheet"
342 configuration in fibrils ³⁵. Misfolded amyloid- β molecules stack perpendicular to the planar
343 surface of the pleated sheet either directly or in a staggering mode. These protofilamentous
344 oligomers display a tertiary "cross- β " conformation and continue to grow into amyloid- β
345 fibers. Nuclear magnetic resonance (NMR) ³⁶ and cryo-electron microscopy (cryo-EM) ³⁷
346 visualized the position and interactions of individual amino acid side chains in the core of
347 *in vitro*-purified amyloid- β fibrils in a single conformation.

348 In the most common proposed model for the amyloid- β misfold, lysine site K28 forms an
349 intramolecular salt bridge with aspartate D23 which stabilizes the hairpin loop which connects
350 the two β -strands³⁸. Amyloid- β fibers can also associate with an alternative number of laterally
351 neighboring fibers which then influence the surface accessibility of lysine K28³⁹. Assuming that
352 A β #K28 is inaccessible for chemical modification in amyloid- β fibers, CPP quantified the relative
353 proportion of fibrillar amyloid- β in AD, and a potentially higher proportion of fibrillar amyloid- β
354 in AD-dLBD patient brain samples. Surprisingly, almost all amyloid- β was fibrillar in a control
355 who was asymptomatic for AD. CPP showed that following ultracentrifugation amyloid- β
356 aggregates displayed fewer molecules with inaccessible A β #K28 than in the initial lysate,
357 suggesting that purifying fibrils might alter one or several different fibrillar amyloid- β
358 conformers. *In vitro* outgrowth assays of amyloid- β fibers seeded with AD patient-derived brain
359 material recently highlighted differences between clinical AD subtypes and the heterogeneity of
360 amyloid- β conformers that can coexist⁴⁰. Furthermore, recent cryo-EM data suggested that
361 A β #K28 can be solvent accessible in distinct strains of amyloid- β fibrils⁴¹⁻⁴³. In addition,
362 denaturation assays revealed up to three different states of amyloid- β aggregation in Alzheimer
363 disease brain samples with up to 4-fold (A β ₁₋₄₀) or 20-fold (A β ₁₋₄₂) more aggregated amyloid- β
364 than soluble amyloid- β ⁴⁴.

365 In conclusion, CPP quantifies the proportion of protein molecules in which a lysine site is
366 accessible for chemical dimethylation in a proteome. With CPP, we determined the
367 contribution of fibrillar amyloid- β with inaccessible A β #K28 in AD and AD-dLBD patient brain
368 samples and revealed that SDHB and TUBB might be conformationally altered upon
369 neurodegeneration.

370

371 Acknowledgements

372 We thank Claire Delahunty for reading the manuscript. We are thankful to Robin Park for
373 support in mass spectrometric data analysis with IP2 (Integrated Proteomics) and Daniel
374 McClatchy for many informal discussions. We thank Ivy Trinh and Jeffery Metcalf from the
375 Rissman laboratory for technical assistance and dissecting brain tissues for this study.

376 Author contributions

377 C.B., S.P. and J.R.Y. designed the research. M.M. performed the GAPDH experiments; S.P. and
378 C.B. performed the HEK293T experiments; C.B. performed the AD experiments and J.D.
379 measured the AD samples on the mass spectrometer. S.M.B. and C.B. conceived and S.M.B.
380 implemented the protein residue-specific quantification and SoPaX in PCQ. R.R. and J.R.Y.
381 provided materials and funding. C.B. wrote the manuscript and prepared the figures with help
382 from all authors. All authors read and approved the manuscript.

383 Competing financial interests

384 The authors do not declare competing financial interests.

385 Funding

386 Funding was provided by NIH grants R03AG047957-02 and R33CA212973-01 awarded to
387 John R. Yates III and funding from the Shiley-Marcos ADRC Neuropathology Core
388 (U19AG010483-26) awarded to Robert A. Rissman.

389 Materials and Methods

390 Chemical Dimethylation of GAPDH

391 A Michael addition reaction was used to dimethylate primary amines. Chemical dimethylation
392 allows the use of different combinations of carbon ^{12}C , and hydrogen H and carbon ^{13}C and
393 Deuterium D in the isotope labels. CPP takes advantage of two successive independent
394 dimethylation reactions to allow for the incorporation of two different isotope-defined
395 dimethyl groups. The specific isotope combination in the first and the second dimethylation
396 step in each of the experiments are listed in Extended data table 5.

397 Dimethylation of GAPDH was performed with recombinantly expressed, highly purified human
398 GAPDH (LifeTechnologies) dissolved in 2 mM HEPES (pH 7.4). In this first step, ϵ -amines of
399 lysine residues were labeled with isotope-defined reagents (H, ^{12}C , “light”) on native
400 proteins. Formaldehyde was in 10-fold molar excess over lysine residues present in the
401 reaction mixture. Specifically, 1.7 μL H_2O , 2.0 μL HEPES buffer pH 7.0 (1 M), 5 μL of GAPDH
402 protein (1 $\mu\text{g}/\mu\text{L}$), 1.7 μL formaldehyde (2 % v:v, Sigma), and 0.6 μL NaBH_3CN (160 mM, Sigma)
403 were mixed (10 μL final) in a small reaction vial, and dimethylation was allowed to proceed for
404 5 min on ice. Following incubation, the reaction was quenched by the addition of ammonium
405 bicarbonate in molar excess (0.5 μL of 0.3 M NH_4HCO_3).

406 Native Gel Electrophoresis

407 Following the initial dimethylation, samples were prepared for native gel electrophoresis by the
408 addition of loading buffer (4 \times NativePage Sample Buffer, Thermo Fisher Scientific) and 1 μg of
409 the GAPDH protein was loaded per lane on a native 4 % to 16 % Bis-Tris gel (NATIVE-PAGE,
410 Thermo). Protein complexes were separated at 15 V/cm in a buffer cooled electrophoresis
411 chamber (Thermo). Gels were fixed in an aqueous solution of 40 % MeOH/10 % acetic acid,
412 microwaved for 45 s and agitated for 30 min at 24 $^\circ\text{C}$. This step was repeated. Gels were
413 subsequently stained (0.02 % Coomassie Blue in 30 % MeOH/10 % acetic acid, BioRad) for
414 30 min at 24 $^\circ\text{C}$ and washed with 8 % acetic acid (30 min at 24 $^\circ\text{C}$). Electrophoretic separation
415 of bovine serum albumin (BSA, Sigma) in an additional sample well facilitated the interpretation

416 of the GAPDH mobility patterns because a GAPDH homo-dimer (71.8 kD) is 5.3 kD heavier than
417 BSA (66.5 kD), and the GAPDH tetramer (145 kD) is more than twice as heavy as BSA.

418 Cell culture and heat shock

419 HEK293T cells were grown under standard conditions (37 °C, 5 % CO₂) in Dulbecco's modified
420 Eagle's medium containing 25 mM Glucose and supplemented with 1 mM Sodium pyruvate,
421 2 mM Glutamax, 10 % FBS and, 1 % Penicillin/Streptomycin (GIBCO). Following heat shock
422 (15 min, 42 °C, 5 % CO₂) cells were immediately labeled with isotope defined reagents
423 (2 % formaldehyde, 0.3 M sodium cyanoborohydride, in 1 × Dulbecco's phosphate buffered
424 saline, pH 7.3) for 15 min at 0 °C. Addition of ammonium bicarbonate (1% final w:v) quenched
425 dimethylation of lysine sites (15 min, 0 °C), cells and cell fragments collected and sonicated for
426 3 min in a water bath sonicator. A methanol-chloroform precipitation according to ⁴⁵ separated
427 proteins from the initial labeling reagents. Precipitated proteins were resolubilized by
428 sonication (1 h) in 1 % Rapigest (Waters), 0.1 M 4-(2-hydroxyethyl)-1-piperazineethanesulfonic
429 acid (HEPES, Gibco), pH 7.5 and heat denatured (95 °C, 10 min). Disulfide bonds were reduced
430 with 5 mM tris-(2-carboxyethyl)phosphine hydrochloride (TCEP, 20 min, 37 °C) and sulfhydryl
431 moieties were alkylated in 10 mM chloroacetamide (30 min, 24 C).

432 Human postmortem brain tissues

433 100 mg of fresh frozen human postmortem frontal cortex from neuropathologically confirmed
434 AD and cognitively normal control cases was obtained from the Neuropathology/Brain Bank of
435 the Shiley-Marcos Alzheimer's Disease Research Center of the University of California, San
436 Diego.

437 Purification of the insoluble brain fraction

438 Purification of the insoluble fraction in brain tissue samples was performed as previously
439 described ¹⁹. In brief, tissue was homogenized in 1 ml tissue lysis buffer (10 % (w:v) sucrose,
440 10 mM HEPES pH 7.0, 800 mM NaCl, 5 mM Ethylenediaminetetraacetic acid (EDTA), 1 mM
441 ethylene glycol-bis(β-aminoethyl ether)-N,N,N',N'-tetraacetic acid (EGTA), 1 × protease
442 inhibitors Complete EDTA-free (Roche), 1 × phosphatase inhibitors (Pierce)) with a small pestle,
443 vigorously mixed (30 s), sonicated (30 s), and tissue debris removed by centrifugation
444 (18,000 × g, 30 min, 4 °C). The cleared tissue lysate supernatant was brought to 1 % N-

445 lauroylsarcosine (v:v), vigorously mixed (30 min, 24 °C), centrifuged (18,000 × g, 30 min,
446 4 °C). Protein aggregates were precipitated from the second supernatant by ultracentrifugation
447 (100,000 × g, 1 h, 4 °C) and the protein pellet was isotope labeled and re-solubilized in one step
448 (2 % formaldehyde, 0.3 M sodium cyanoborohydride, in 100 mM Hepes pH 7.0, 10 µl final
449 volume, vigorously mixing, 15 min, 24 °C). The dimethylation reaction was quenched with
450 ammonium bicarbonate (1% final w:v, 5 min, 24 °C). Proteins were denatured (8 M guanidinium
451 chloride, 10 mM TCEP) for 1 h at 37 °C and free sulfhydryl moieties alkylated
452 (20 mM iodoacetamide, 30 min, 24 °C).

453 Enzymatic digestion and second labeling step

454 Only brain samples were diluted to 1 M guanidinium chloride in 0.1 mM HEPES, pH 8.0, 0.02 %
455 Rapigest. All samples were heat denatured (5 min, 95 °C), and proteins were digested with the
456 endoprotease Chymotrypsin at either 5 µg/ml (w:v, brain samples, 16 h, 37 °C) or at a 1: 100
457 ratio of protease : protein (w:w, GAPDH and HEK293T samples, 16 h, 30 °C).

458 Rapigest was inactivated by acidification (1 % v:v, 37 °C, 1 h) and the insoluble precipitate
459 removed by centrifugation (18,000 × g, 15 min, 4 °C) in brain-derived or GAPDH
460 samples. Peptides were desalted by C18 reversed phase purification (C18-tips, Thermo Fisher
461 Scientific) to remove residual reagents from the first labeling step. While still bound to the
462 resin newly exposed primary amines on peptides were dimethylated with isotope-defined
463 reagents (2 % formaldehyde, 0.3 M sodium cyanoborohydride, in 100 mM HEPES, pH 7.0,
464 occasional mixing, 15 min, 24 °C) as previously described⁴⁶. Peptides were eluted with 80 %
465 acetonitrile, 0.01 % trifluoroacetic acid. The eluted samples were evaporated almost to dryness
466 by centrifugation under vacuum, and peptides were resolubilized in liquid chromatography
467 buffer A (5 % acetonitrile, 0.1 % formic acid).

468 For proteins that were methanol-chloroform precipitated, peptides were directly labeled with
469 isotope defined reagents (2 % formaldehyde, 0.3 M sodium cyanoborohydride, in 100 mM
470 HEPES, pH 7.0, occasional mixing, 1 h, 24 °C). Rapigest was inactivated by acidification (1 % v:v,
471 37 °C, 1 h), and samples reduced to near dryness *in vacuo* as described above, and finally
472 resolubilized in liquid chromatography buffer A (5 % acetonitrile, 0.1 % formic acid).

473 Mass spectrometry

474 In all experiments, peptides were electrospray ionized at a nano-spray tip of ~0.1 µm i.d. at
475 1.5 kV. Full scan (400 to 1800 m/z) spectra were acquired on an Orbitrap mass spectrometer
476 (Thermo Fisher Scientific) at a resolution 60,000. Fragment ion spectra of > 1000 ion counts
477 were acquired in data dependent mode for the top 20 highest intense selected ions (z = 2 or
478 higher) with collision-induced dissociation (CID) at 35% collisional energy and recorded in the
479 linear ion trap detector of the mass spectrometer. To avoid sampling only the most abundant
480 peaks, dynamic exclusion with an exclusion list of 500, repeat time of 60 s and asymmetric
481 exclusion window of -0.51 Da and +1.50 Da was used throughout all experiments.

482 In each experiment samples were chromatographically separated using different methods and
483 mass spectra acquired at different Orbitrap mass spectrometers. Specifically, 250 ng of GAPDH
484 peptides were loaded onto a 300 mm reversed phase chromatographic column with 100 µm
485 inner diameter packed with 100 Å reversed phase resin (Aqua 3, 10 Å pore size,
486 Phenomenex). A linear chromatographic gradient of 100 % buffer A (5% Acetonitrile, 0.1 %
487 formic acid) to 60 % buffer B (80 % acetonitrile, 0.1 % formic acid) was applied over 1.5 h to
488 elute peptides. Mass spectra were acquired with an Orbitrap Fusion mass spectrometer
489 (Thermo Fisher Scientific).

490 For the heat shock experiment, 50 µg of the CPP labeled HEK293T proteome was loaded onto a
491 MudPIT column¹⁷ and analyzed by nano-ESI LC/LC-MS/MS on a VelosPro Orbitrap mass
492 spectrometer. The MudPIT column was placed in line with a quaternary Agilent 1200 high
493 pressure liquid chromatography HPLC pump and peptides were separated by reversed phase
494 liquid chromatography in 10 sequential steps, each following an initial elution of peptides from
495 the strong cation exchange column with buffer C (500 mM ammonium acetate, 5 % acetonitrile,
496 0.1 % formic acid) in buffer A in incrementally progressive concentrations (0 %, 10 %, 20 %, 30 %, 40 %, 50 %, 60 %, 70 %, 80 %, and 90 %) as described previously^{17,47}.

498 For patient samples, 2 µg of brain sample derived peptides were loaded onto evotip C18 tips
499 according to the manufacturer's protocol (EVOSEP, Denmark). Peptides were eluted from the
500 evotip with an EVOSEP HPLC system (EVOSEP, Denmark) and separated by reversed phase
501 chromatography on a 15 cm ReproSil C18 column (3 µm, 120 Å, id 100 µm, PepSep, Denmark)

502 with a 45 min gradient of increasing Acetonitrile concentration with 0.1% formic acid according
503 to manufacturer's recommendations. Following chromatographic separation, peptides were
504 transferred into an Orbitrap Lumos mass spectrometer by electrospray ionization (nanoEasy,
505 Thermo Fisher Scientific). The top 25 precursor peaks were picked for collision-induced
506 fragmentation.

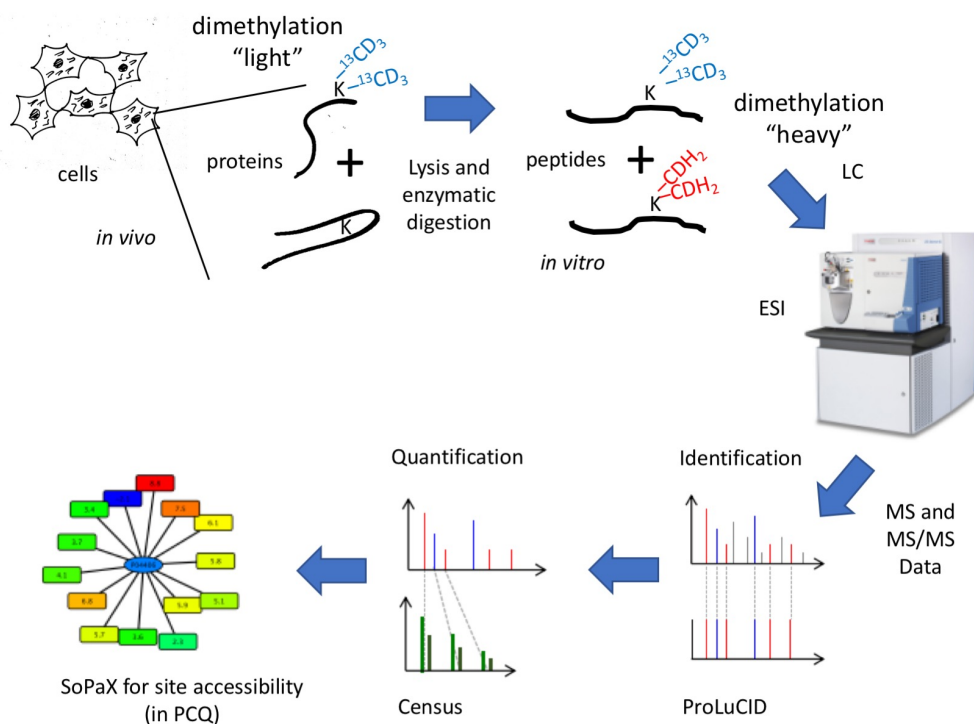
507 Data analysis

508 Following data acquisition, raw data was pre-processed and converted into ASCII file format
509 with *RawConverter*⁴⁸ set to monoisotopic peak detection. Converted files were uploaded in *IP2*
510 (Integrated Proteomics) and searched with *ProLuCID*⁴⁹ for the presence of spectra that
511 matched a theoretical peptide fragment ion spectrum based on amino acid sequences listed in
512 the UniProt database for the human proteome release v 2016.4. Amino acid sequences in the
513 database were either digested *in silico* assuming either no endoproteolytic enzyme specificity
514 (HEK293T cells) or minimally requiring that either the N- or C-terminus of the peptide was
515 generated by chymotryptic cleavage (GAPDH and brain samples). A 50 ppm precursor mass
516 tolerance window was set for peptide candidate selection, carboxyamidomethylation
517 ($m = 57.021464$ Da) of cysteine, and dimethylation ($m = 28.0313$ Da) of N-termini. Peptides
518 including lysine residues labeled "light" or "heavy" (+8.0442 Da) were searched separately as
519 static modifications. Results were filtered with DTASelect v 2.1.4 to a spectrum false discovery
520 rate (FDR) of 0.1 % or less and requiring at least one Chymotrypsin specific cleavage of either
521 peptide N- or C-terminus and a precursor mass tolerance of $\Delta \leq \pm 10$ ppm. Subsequently,
522 relative peptide abundances were quantified based on peptide elution profiles deduced from
523 MS survey spectra with Censu¹⁵ in IP2 (Integrated Proteomics) or based on fragment ion
524 counting in case isotopically labeled peptides were isobaric¹³. Ratio values for each lysine
525 residue were calculated with the SoPaX algorithm that is part of ProteinClusterQuant⁵⁰ (PCQ,
526 <https://github.com/proteomicsyates/ProteinClusterQuant>),. Data presentations were
527 assembled in Excel (Microsoft) or in Prism (GraphPad) to determine the FDR of lysine sites in
528 two sample comparisons according to the modified statistical approach originally proposed by
529 Benjamini and Hochberg⁵¹. Panther⁵² determined the Gene ontology enrichment of protein
530 groups.

531 Crystal structures of proteins were downloaded from the RCSB Protein Data Bank PDB
532 (<https://www.rcsb.org/pdb/home/home.do>) and visualized in Jmol (v 14.19.1). All non-protein
533 molecules and hydrogen atoms were removed. Based on the van der Waals spheres of
534 individual atoms the command *isosurface* in Jmol determined the solvent accessible surface
535 (SASA) at the reactive ϵ -amine of each lysine residue with standard parameter settings (probe
536 radius 1.2 Å and 2 points per Å resolution). Euclidian distances of atoms were determined with
537 the function *distance dependent contacts of one residue with polar residues* that is available in
538 the WHAT IF web interface (<http://swift.cmbi.ru.nl/servers/html/index.html>) or with the
539 ProteinAssessibilityCalculator (PAC,
540 <https://github.com/proteomicsyates/ProteinAssessibilityCalculator>).

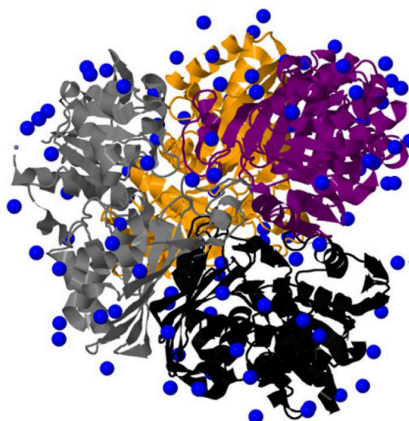
541 Extended data

542 Extended data figures



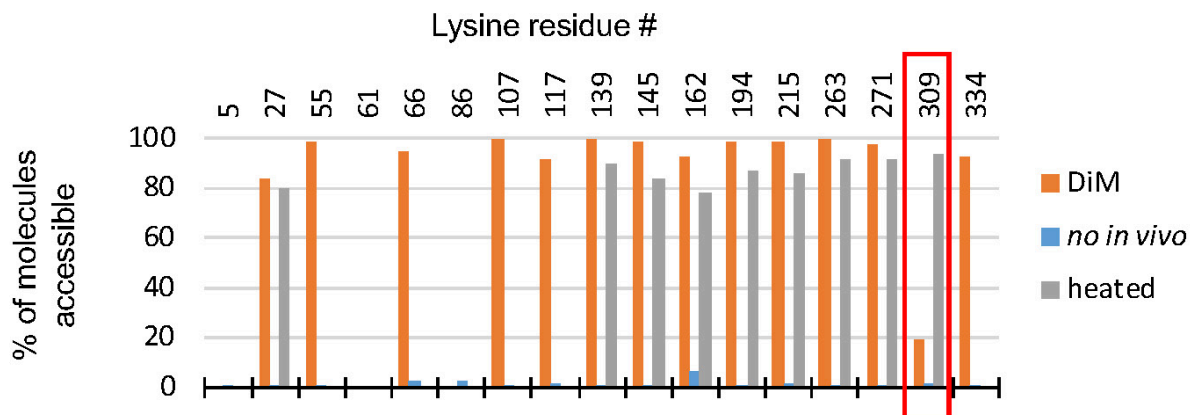
543
 544 **Extended data figure 1: Schematic of the CPP method.** CPP includes *in vivo* chemical methylation of lysine residues at the
 545 surface of proteins and its detection with mass spectrometry. The flow chart shows each labeling step and the resultant relative
 546 measurement of surface accessibility for chemical modification based on mass spectrometric quantification of isotope labeled
 547 peptides. Proteins are labeled with isotope defined reagents at solvent exposed lysine residues (K) with two methyl moieties ($^{13}\text{CD}_3$,
 548 heavy) *in vivo*. Protein are then digested in peptides with the endoproteinase Chymotrypsin, and all newly accessible primary
 549 amines labeled with two methyl moieties (CH_3 , light). Peptides are separated by liquid chromatography (LC) and transferred into
 550 gas phase by electrospray ionization (nano ESI). High mass resolution (Orbitrap) mass spectra (MS) and fragment ion mass
 551 spectra (MS/MS) are acquired. Peptides are identified with a database search using ProLuCID and quantified with Census. The
 552 "surfaces of all protein complexes" (SoPaX) algorithm within ProteinClusterQuant (PCQ) determines and compares the relative
 553 surface accessibility of lysine residues.

554



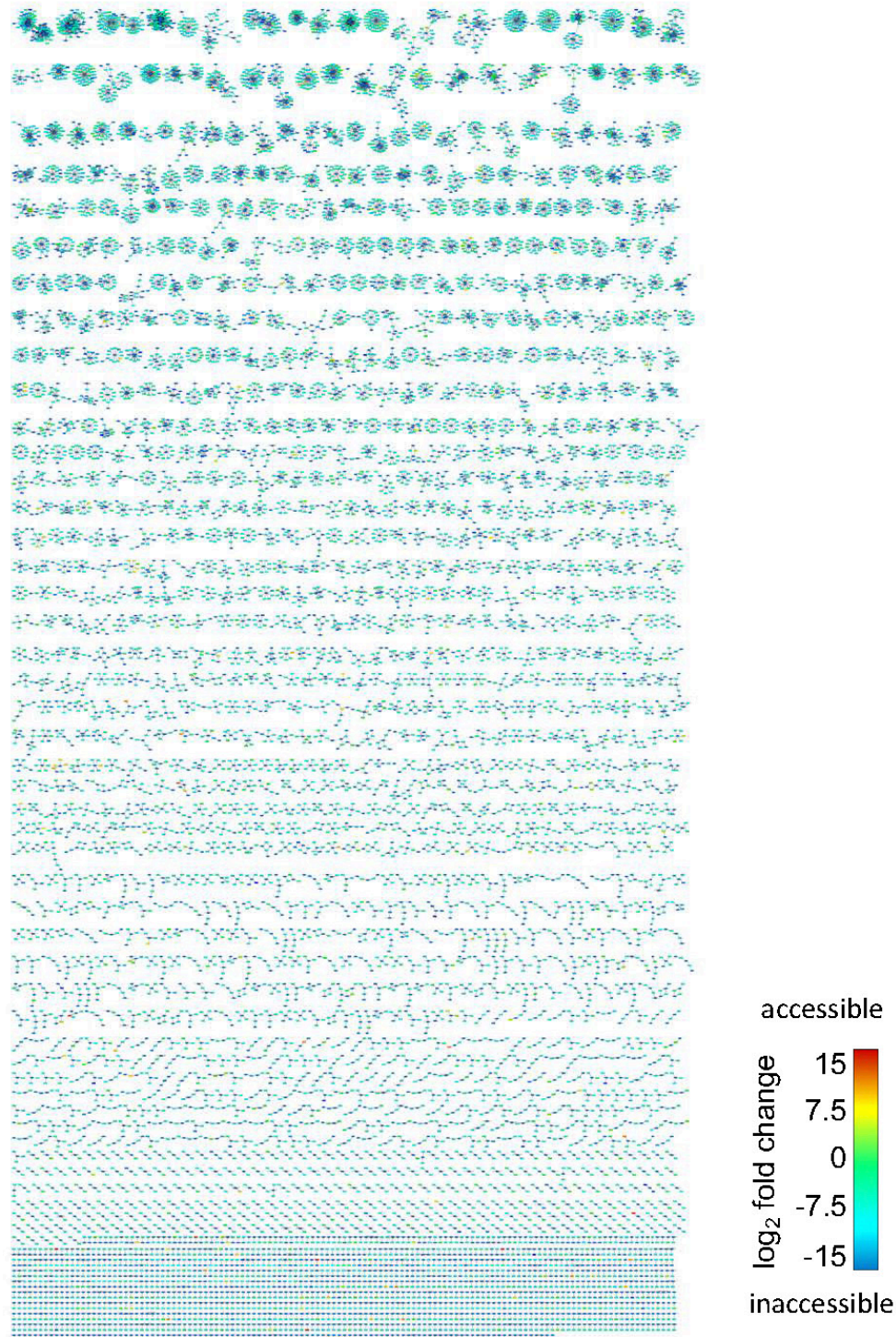
555 **Extended data figure 2: Tetrameric structure of GAPDH with the ϵ -amine of all lysine residues highlighted with blue**
556 **spheres.** Blue dots indicate the location of each lysine ϵ -amine relative to the ribbon fold of GAPDH subunits A (yellow), B (purple),
557 C (grey), and D (black) in the GAPDH homo-tetramer (PDB: 4wnc¹⁴).

558



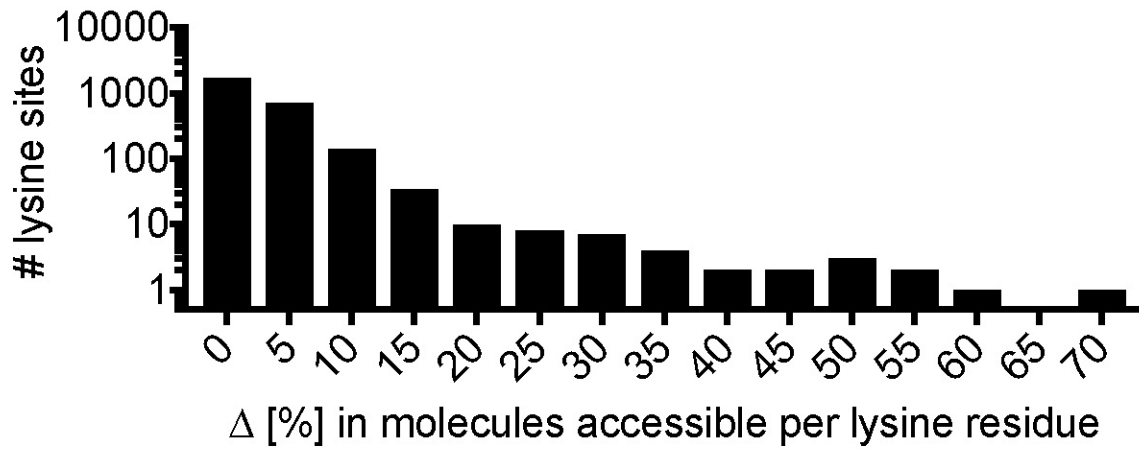
559 **Extended data figure 3: Relative accessibility of lysine residues for chemical modification expressed in percent of**
560 **molecules.** The bar graph shows the same set of measurements as in Figure 1D with the ratio value converted to a percentage of
561 the total amount of lysine residues that were available during the initial labeling step, which is the percentage of GAPDH protein
562 molecules in which the lysine residue was accessible for chemical modification. Orange bars represent relative surface
563 accessibilities determined by standard labeling dimethylation conditions ("DiM"). In addition, GAPDH was heat denatured and
564 subsequently labeled (grey, "heated"), or the initial labeling step was omitted and only peptides were labeled following endo-
565 proteolytic digestion of GAPDH (blue, "no light labeling"). Measurements for lysine residue GAPDH#K309 are highlighted with a red
566 box.

567



568 **Extended data figure 4: Protein-peptide representation of all lysine residues identified and quantified in HEK293T**
569 **cells.** The bipartite network shows all lysine-harboring peptides (rectangles) to protein (ellipses) relationships as edges that were
570 identified with CPP in HEK293T cells. The color of each peptide node reflects the relative molar accessibility of each lysine residue
571 according to the color scale indicted on the lower right. The predominant color turquoise in the network graph shows that most
572 lysine residues are accessible in the majority of protein molecules.

573



574 Extended data figure 5: The frequency plot shows the number of lysine residues (y-axis) that alter in surface accessibility
575 per binned percent of protein molecules (percent bin is 5, x-axis).

576 Extended data network

577 **Extended data Network 1: The protein-peptide network of control HEK293T cells shown.** The
578 bipartite network in Extended data figure 4 is available on NDEx with the following URL:

579 <http://www.ndexbio.org/#/network/dc5d06ab-fa49-11e7-adc1->

580 [0ac135e8bacf?accesskey=cbac0a4309d1dc09f5c7dab3be90923e39d7a98616bf64f5ba58feb95f](http://www.ndexbio.org/#/network/dc5d06ab-fa49-11e7-adc1-0ac135e8bacf?accesskey=cbac0a4309d1dc09f5c7dab3be90923e39d7a98616bf64f5ba58feb95f)

581 [5f88a7](http://www.ndexbio.org/#/network/dc5d06ab-fa49-11e7-adc1-0ac135e8bacf?accesskey=cbac0a4309d1dc09f5c7dab3be90923e39d7a98616bf64f5ba58feb95f)

582 Extended data tables

583 **Extended data table 1: Surface accessibility measurements with CPP for lysine residues in**
584 **HEK293T cells using isobaric methyl moieties.**

585 **Extended data table 2: Surface accessibility measurements with CPP for lysine residues in**
586 **heat shock and control HEK293T cells.**

587 **Extended data table 3: Significantly different sites in HEK293T cells following heat shock.**

588 **Extended data table 4: Patient diagnosis of human brain samples.** Abbreviations: PM,
589 *postmortem*; BLES, Blessed Orientation-Memory-Concentration Test; MMSE, mini mental state
590 exam; DRS, dementia rating scale.

591 **Extended data table 5: Isotope combinations selected for labeling in CPP.** The list denotes
592 the experiment and the isotope combination chosen for the first and second labeling step in
593 CPP.

594 **Data Availability:** Mass spectrometric raw data, search engine result files, and quantification
595 result files can be accessed in Massive or ProteomeXchange (MassIVE MSV000083031,
596 ProteomeXchange PXD011351).

597 Bibliography

- 598 1 Zlokovic, B. V. Neurovascular pathways to neurodegeneration in Alzheimer's disease and
599 other disorders. *Nat Rev Neurosci* **12**, 723-738, (2011).
- 600 2 Scheltens, P. *et al.* Alzheimer's disease. *Lancet* **388**, 505-517, (2016).
- 601 3 Balch, W. E., Morimoto, R. I., Dillin, A. & Kelly, J. W. Adapting proteostasis for disease
602 intervention. *Science* **319**, 916-919, (2008).
- 603 4 Adhikari, J., West, G. M. & Fitzgerald, M. C. Global analysis of protein folding
604 thermodynamics for disease state characterization. *Journal of proteome research* **14**,
605 2287-2297, (2015).
- 606 5 West, G. M., Tang, L. & Fitzgerald, M. C. Thermodynamic analysis of protein stability and
607 ligand binding using a chemical modification- and mass spectrometry-based strategy.
608 *Analytical chemistry* **80**, 4175-4185, (2008).
- 609 6 Harlow, E. & Lane, D. *Using antibodies : a laboratory manual*. (Cold Spring Harbor
610 Laboratory Press, 1999).
- 611 7 Kahsai, A. W. *et al.* Multiple ligand-specific conformations of the beta2-adrenergic
612 receptor. *Nat Chem Biol* **7**, 692-700, (2011).
- 613 8 Zhou, Y. & Vachet, R. W. Diethylpyrocarbonate labeling for the structural analysis of
614 proteins: label scrambling in solution and how to avoid it. *Journal of the American
615 Society for Mass Spectrometry* **23**, 899-907, (2012).
- 616 9 Zhou, Y. & Vachet, R. W. Covalent labeling with isotopically encoded reagents for faster
617 structural analysis of proteins by mass spectrometry. *Analytical chemistry* **85**, 9664-
618 9670, (2013).
- 619 10 Kallen, R. G. & Jencks, W. P. Equilibria for the reaction of amines with formaldehyde and
620 protons in aqueous solution. A re-examination of the formol titration. *The Journal of
621 biological chemistry* **241**, 5864-5878, (1966).
- 622 11 Luchini, A., Espina, V. & Liotta, L. A. Protein painting reveals solvent-excluded drug
623 targets hidden within native protein-protein interfaces. *Nat Commun* **5**, 4413, (2014).
- 624 12 Schopper, S. *et al.* Measuring protein structural changes on a proteome-wide scale using
625 limited proteolysis-coupled mass spectrometry. *Nature protocols* **12**, 2391-2410, (2017).
- 626 13 Bamberger, C., Pankow, S., Park, S. K. & Yates, J. R., 3rd. Interference-free proteome
627 quantification with MS/MS-based isobaric isotopologue detection. *Journal of proteome
628 research* **13**, 1494-1501, (2014).
- 629 14 White, M. R. *et al.* A dimer interface mutation in glyceraldehyde-3-phosphate
630 dehydrogenase regulates its binding to AU-rich RNA. *The Journal of biological chemistry*
631 **290**, 1770-1785, (2015).
- 632 15 Park, S. K., Venable, J. D., Xu, T. & Yates, J. R., 3rd. A quantitative analysis software tool
633 for mass spectrometry-based proteomics. *Nature methods* **5**, 319-322, (2008).
- 634 16 Ben-Zvi, A., Miller, E. A. & Morimoto, R. I. Collapse of proteostasis represents an early
635 molecular event in *Caenorhabditis elegans* aging. *Proceedings of the National Academy
636 of Sciences of the United States of America* **106**, 14914-14919, (2009).
- 637 17 Washburn, M. P., Wolters, D. & Yates, J. R., 3rd. Large-scale analysis of the yeast
638 proteome by multidimensional protein identification technology. *Nature biotechnology*
639 **19**, 242-247, (2001).

- 640 18 Golebiowski, F. *et al.* System-wide changes to SUMO modifications in response to heat
641 shock. *Sci Signal* **2**, ra24, (2009).
- 642 19 Goedert, M., Spillantini, M. G., Cairns, N. J. & Crowther, R. A. Tau proteins of Alzheimer
643 paired helical filaments: abnormal phosphorylation of all six brain isoforms. *Neuron* **8**,
644 159-168, (1992).
- 645 20 Karran, E., Mercken, M. & De Strooper, B. The amyloid cascade hypothesis for
646 Alzheimer's disease: an appraisal for the development of therapeutics. *Nat Rev Drug*
647 *Discov* **10**, 698-712, (2011).
- 648 21 Khoshnevis, S. *et al.* The DEAD-box Protein Rok1 Orchestrates 40S and 60S Ribosome
649 Assembly by Promoting the Release of Rrp5 from Pre-40S Ribosomes to Allow for 60S
650 Maturation. *PLoS Biol* **14**, e1002480, (2016).
- 651 22 Young, C. L. & Karbstein, K. The roles of S1 RNA-binding domains in Rrp5's interactions
652 with pre-rRNA. *RNA* **17**, 512-521, (2011).
- 653 23 Coccia, M., Rossi, A., Riccio, A., Trotta, E. & Santoro, M. G. Human NF-kappaB repressing
654 factor acts as a stress-regulated switch for ribosomal RNA processing and nucleolar
655 homeostasis surveillance. *Proceedings of the National Academy of Sciences of the United*
656 *States of America* **114**, 1045-1050, (2017).
- 657 24 Duda, D. M. *et al.* Structure of a glomulin-RBX1-CUL1 complex: inhibition of a RING E3
658 ligase through masking of its E2-binding surface. *Molecular cell* **47**, 371-382, (2012).
- 659 25 Kaneko, I., Yamada, N., Sakuraba, Y., Kamenosono, M. & Tutumi, S. Suppression of
660 mitochondrial succinate dehydrogenase, a primary target of beta-amyloid, and its
661 derivative racemized at Ser residue. *J Neurochem* **65**, 2585-2593, (1995).
- 662 26 Klinger, A. L. *et al.* A synchrotron-based hydroxyl radical footprinting analysis of amyloid
663 fibrils and prefibrillar intermediates with residue-specific resolution. *Biochemistry* **53**,
664 7724-7734, (2014).
- 665 27 Li, K. S., Rempel, D. L. & Gross, M. L. Conformational-Sensitive Fast Photochemical
666 Oxidation of Proteins and Mass Spectrometry Characterize Amyloid Beta 1-42
667 Aggregation. *J Am Chem Soc* **138**, 12090-12098, (2016).
- 668 28 Gau, B. C., Sharp, J. S., Rempel, D. L. & Gross, M. L. Fast photochemical oxidation of
669 protein footprints faster than protein unfolding. *Analytical chemistry* **81**, 6563-6571,
670 (2009).
- 671 29 Scheraga, H. A. Deuterium exchange studies and protein structure. *Brookhaven Symp*
672 *Biol* **13**, 71-88, (1960).
- 673 30 Williams, A. D. *et al.* Structural properties of Abeta protofibrils stabilized by a small
674 molecule. *Proceedings of the National Academy of Sciences of the United States of*
675 *America* **102**, 7115-7120, (2005).
- 676 31 Ramos, I., Fabris, D., Qi, W., Fernandez, E. J. & Good, T. A. Kinetic study of beta-amyloid
677 residue accessibility using reductive alkylation and mass spectrometry. *Biotechnol*
678 *Bioeng* **104**, 181-192, (2009).
- 679 32 Iwata, K., Eyles, S. J. & Lee, J. P. Exposing asymmetry between monomers in Alzheimer's
680 amyloid fibrils via reductive alkylation of lysine residues. *J Am Chem Soc* **123**, 6728-6729,
681 (2001).
- 682 33 Terry, R. D., Gonatas, N. K. & Weiss, M. Ultrastructural Studies in Alzheimer's Presenile
683 Dementia. *Am J Pathol* **44**, 269-297, (1964).

- 684 34 Cohen, A. S. & Calkins, E. Electron microscopic observations on a fibrous component in
685 amyloid of diverse origins. *Nature* **183**, 1202-1203, (1959).
- 686 35 Eanes, E. D. & Glenner, G. G. X-ray diffraction studies on amyloid filaments. *J Histochem*
687 *Cytochem* **16**, 673-677, (1968).
- 688 36 Barrow, C. J. & Zagorski, M. G. Solution structures of beta peptide and its constituent
689 fragments: relation to amyloid deposition. *Science* **253**, 179-182, (1991).
- 690 37 Sachse, C., Fandrich, M. & Grigorieff, N. Paired beta-sheet structure of an Abeta(1-40)
691 amyloid fibril revealed by electron microscopy. *Proceedings of the National Academy of*
692 *Sciences of the United States of America* **105**, 7462-7466, (2008).
- 693 38 Petkova, A. T. *et al.* A structural model for Alzheimer's beta -amyloid fibrils based on
694 experimental constraints from solid state NMR. *Proceedings of the National Academy of*
695 *Sciences of the United States of America* **99**, 16742-16747, (2002).
- 696 39 Paravastu, A. K., Leapman, R. D., Yau, W. M. & Tycko, R. Molecular structural basis for
697 polymorphism in Alzheimer's beta-amyloid fibrils. *Proceedings of the National Academy*
698 *of Sciences of the United States of America* **105**, 18349-18354, (2008).
- 699 40 Qiang, W., Yau, W. M., Lu, J. X., Collinge, J. & Tycko, R. Structural variation in amyloid-
700 beta fibrils from Alzheimer's disease clinical subtypes. *Nature* **541**, 217-221, (2017).
- 701 41 Walti, M. A. *et al.* Atomic-resolution structure of a disease-relevant Abeta(1-42) amyloid
702 fibril. *Proceedings of the National Academy of Sciences of the United States of America*
703 **113**, E4976-4984, (2016).
- 704 42 Schmidt, A., Annamalai, K., Schmidt, M., Grigorieff, N. & Fandrich, M. Cryo-EM reveals
705 the steric zipper structure of a light chain-derived amyloid fibril. *Proceedings of the*
706 *National Academy of Sciences of the United States of America* **113**, 6200-6205, (2016).
- 707 43 Gremer, L. *et al.* Fibril structure of amyloid-beta(1-42) by cryo-electron microscopy.
708 *Science* **358**, 116-119, (2017).
- 709 44 Cohen, M. L. *et al.* Rapidly progressive Alzheimer's disease features distinct structures of
710 amyloid-beta. *Brain* **138**, 1009-1022, (2015).
- 711 45 Pankow, S., Bamberger, C., Calzolari, D., Bamberger, A. & Yates, J. R., 3rd. Deep
712 interactome profiling of membrane proteins by co-interacting protein identification
713 technology. *Nature protocols* **11**, 2515-2528, (2016).
- 714 46 Boersema, P. J., Raijmakers, R., Lemeer, S., Mohammed, S. & Heck, A. J. Multiplex
715 peptide stable isotope dimethyl labeling for quantitative proteomics. *Nature protocols*
716 **4**, 484-494, (2009).
- 717 47 Pankow, S. *et al.* F508 CFTR interactome remodelling promotes rescue of cystic fibrosis.
718 *Nature* **528**, 510-516, (2015).
- 719 48 He, L., Diedrich, J., Chu, Y. Y. & Yates, J. R., 3rd. Extracting Accurate Precursor
720 Information for Tandem Mass Spectra by RawConverter. *Analytical chemistry* **87**, 11361-
721 11367, (2015).
- 722 49 Xu, T. *et al.* ProLuCID: An improved SEQUEST-like algorithm with enhanced sensitivity
723 and specificity. *J Proteomics* **129**, 16-24, (2015).
- 724 50 Bamberger, C. *et al.* Deducing the presence of proteins and proteoforms in quantitative
725 proteomics. *Nat Commun* **9**, 2320, (2018).
- 726 51 Reiner, A., Yekutieli, D. & Benjamini, Y. Identifying differentially expressed genes using
727 false discovery rate controlling procedures. *Bioinformatics* **19**, 368-375, (2003).

728 52 Mi, H., Muruganujan, A., Casagrande, J. T. & Thomas, P. D. Large-scale gene function
729 analysis with the PANTHER classification system. *Nature protocols* **8**, 1551-1566, (2013).
730